Synthesis of the Battery Charging System of a Stand-Alone Electric Locomotive

Alexandru Bitoleanu[1], Mihaela Popescu[1],Vlad Constantin Suru[1] and Mihail Radulescu[2]
[1]University of Craiova/Electromechanical, Environmental and Applied Informatics Department, Craiova, Romania,
alex.bitoleanu@em.ucv.ro, mpopescu@em.ucv.ro, vsuru@em.ucv.ro
[2]SC INDA SRL, Craiova, Romania, mihai.radulescu@inda.ro

***Abstract* - The paper presents the synthesis of the battery charging system of an electric stand-alone locomotive. The traction converter as boost rectifier is used together with a dedicated control strategy in order to obtain the unity power factor on the grid. Two objectives, often contradictory, that can be tracked in the choice of the control mode for the PWM rectifier are highlighted: increasing the performance, in order to obtain a rectifier with the best power factor, the best-controlled load current, acceptable switching frequencies for common power transistors, a stable operation of the control system, etc.; reducing the complexity and price of the converter by giving up certain elements of the control system, such as the multiplication circuit, the voltage loop, and the use of specialized integrated circuits. A patented structure which responds better to the requirements and particularities of autonomous vehicles is used. In the control part, direct current control method is adopted and it was implemented by two control loops. The external loop is dedicated to charging current control and the internal loop is dedicated to grid current control. In order to the performance determination, the entire system is analyzed under Simulink environment and the energetic performances are determined. Also, the influence of switching frequency is analyzed.**

Cuvinte cheie: *încărcare baterie, redresor pwm, controlul direct al curentului, regulator PI, criteriul modulului.*

Keywords: *battery charging, pwm rectifier, direct current control, PI controller, modulus criterion.*

I. INTRODUCTION

In the case of self-powered electric vehicles with induction motors, the traction converter can be controlled in the PWM rectifier mode and used to charge the battery. The control scheme must provide three objectives [3] - [9]:

a) stable and rigorous control of the charging current of the battery; b) control of the current absorbed by the grid to maximize the power factor; c) stabilizing the output voltage.

The first two of these objectives are mandatory and determinant for the system performance, since both have a decisive contribution to generating the reference current wave. Thus, the amplitude is fixed by the stabilizing function, and the sinusoidal shape and phase are fixed by the objective of reaching unity power factor.

As for the third, it has little influence on energy performance because the effects of a variable voltage across a wide range can be considerably diminished by an appropriate control.

The paper is one result of POC project no. 76/2016.

Many control methods for regenerative rectifiers are known, each of them with advantages and drawbacks.

A relatively recent control method is based on the synchronverter technology, which involves controling the rectifier so that it mimics the operation of a synchronous motor (synchronous compensator) [13].

Another method that can be used to control the regenerative PWM rectifiers is the phasorial modulation, widely used in the control of the asynchronous motors actuators and voltage inverters [14].

Generally, the control algorithm involves the use of an internal loop to adjust the current absorbed by the rectifier from the network. Also, other external loops are used to adjust variables quantities, such as output voltage, power factor etc. The use of the phasorial modulation involves phase voltage control on the rectifier interface filter in the fixed orthogonal reference or in the rotating orthogonal reference. The use of the latter is more advantageous, because the projections of the alternative quantities on the orthogonal axes will become DC quantities [12].

This paper presents the synthesis of the battery charging system of an electric stand-alone locomotive and it is organized on six sections. After a short presentation of the power structure, section III is dedicated to describe the control part based on direct current control. Next, the transfer functions are found and the tuning of PI current controller using the modulus criterion in Kesller variant is presented. In section V, the performances of the system are presented and commented. Finally, few conclusions and remarks are drawn.

II. THE STRUCTURE OF POWER PART

Due to its bidirectional energy flow character, the regenerative rectifier is very useful in asynchronous motor drive systems with frequency static converters for autonomous electric vehicles (Fig. 1). There are two specific aspects of this application.

1. The engine can operate in regenerative braking mode, the braking energy being taken from the intermediate DC circuit and used to charge the batteries;

2. When the vehicle is at rest, by supplying the inverter on the AC-side, it can act as a rectifier and absorb power from the grid to charge the batteries.

A more economical structure which responds better to the requirements and particularities of autonomous vehicles is that described in [11] (Fig. 1.b). Compared to the structure of Fig. 1.a, the additional inductance LF is replaced by the inductance of the traction motor windings, thus ensuring the minimization of masses and costs, as well as the simplification of the loading station, which is

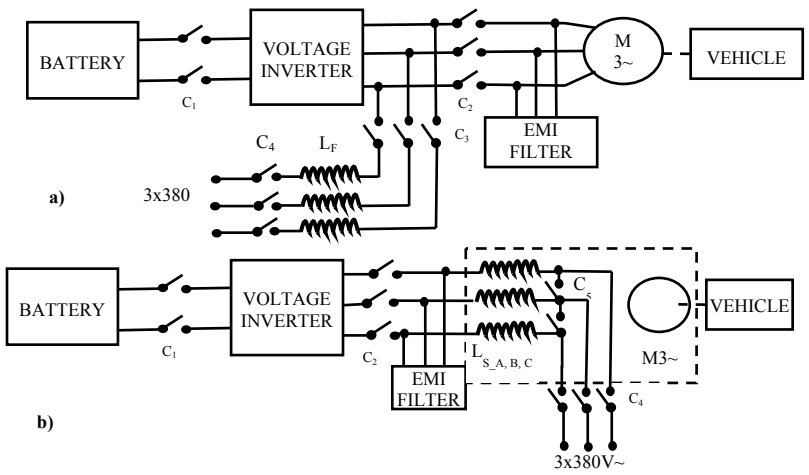

Fig. 1. Variants of use the traction inverter of an autonomous vehicle to charge the battery: a) with additional energy storage (L_F); b) using stator coils as an energy accumulator.

reduced to a simple three-phase source available virtually anywhere. It gives more freedom of movement of the stand-alone vehicle without imposing a specific route related to the locations of special loading stations.

III. The Control Part

A. *Direct current control*

The control system of a PWM rectifier must have a current regulating loop whose output determines the control sequences of the transistors [4]. The direct current control involves adjusting the current to the AC grid [1], [2].

The authors' research has shown that there is a perfect analogy between the operation in regenerative mode of a parallel active filter [1], [2] and the operation of a boost PWM rectifier. It follows that the most appropriate control method is the direct control based on the voltage/DC current controller output. The main advantage of the direct current control is its simplicity (Fig. 2). Consequently, the performance can also be very good if the following conditions are met:

1. The block generating the sine wave waveforms of the grid voltage (Voltage Wave) is correctly synthesized; for immunity to the real voltage distortion, a PLL loop [10] can be adopted, containing a PI regulator;

2. The voltage regulator is correctly synthesized;

3. Rectifier transistors support switching frequencies in the range of (5-10) kHz and a proper interface circuit is placed between grid and rectifier [12], [15].

The current regulator can be of PI type, with hysteresis or other structure (fuzzy, predictive etc.).

If the controller is of the PI type, the control signals are obtained by comparing its output with a modulating signal that determines the switching frequency (Fig. 3). Although PI type controllers followed by the PWM modulator have the advantage of maintaining a constant switching frequency of the transistors and they are frequently dealt with in the literature, the difficulty of achieving the desired current makes this control solution to be rarely adopted in practical applications.

The hysteresis controllers are the simplest; they also contain a PWM modulator, but operate with variable switching frequency, depending on the load current dynamics.

It is worth pointing out that, in reality, the switching frequency in the case of the hysteresis controllers is maximum at zero current (when the current has the maximum variation speed) and has a minimum value when the current (assumed with sinusoidal shape) has a maximum value. An approximate relationship between the hysteresis threshold (Δi), the peak current value (I_M) and the maximum switching frequency of the current over one phase (f_{swM}) can be established as follows:

$$\Delta i = \frac{\omega I_M}{f_{swM}} \tag{1}$$

On this basis, the hysteresis band can be imposed so that the maximum switching frequency is not exceeded.

B. *Generating the waveform of the grid current*

For the calculation of the prescribed grid current, the generation of three sine wave signals with unity magnitude is required.

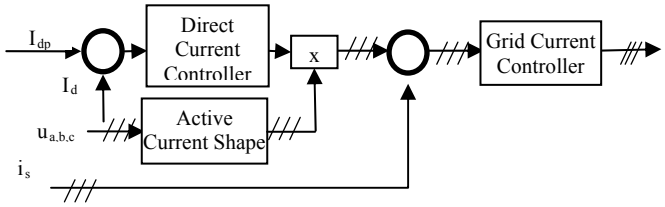

Fig. 2. Block diagram of the direct current control.

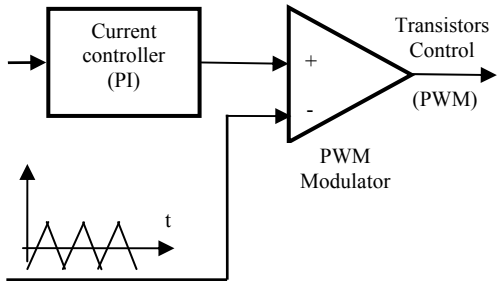

Fig. 3. Structure of the PI Current controller with PWM Modulator.

These signals are the patterns of the active phase currents and their generation depends fundamentally on the waveforms of the power supply voltages.

Thus, if the supply voltages are sinusoidal, these templates can be obtained directly from the phase voltages by dividing them by their amplitudes.

There are two aspects that need to be taken into account, because they occur in the synthesis of the control algorithm:

1. If the amplitude of the power supply voltage does not vary by more than 10% relative to the nominal value, the nominal amplitude value can be used, as the effects of the variations can be compensated by the controller located upstream of the grid current control loop;
2. If the amplitude of the power supply voltage varies by more than 10% relative to the nominal value, the dividing voltage value is calculated by direct peak value detection or by calculating the mean value of the phase voltages.

The first way introduces a T/2 delay because the maximum value detection is discreet at intervals of at least T/2, where T is the supply voltage period.

The second way is to consider the instantaneous value of the mean value calculated with the following relationship:

$$U_{AV} = \frac{2}{T}\int_{t-T/2}^{t} |u_{a,b,c}|\,dt \qquad (2)$$

Then, the peak value corresponds to a sinusoidal quantity, respectively:

$$U_V = \frac{\pi}{2} U_{AV} \qquad (3)$$

If the voltage is not sinusoidal, the patterns of the active currents are obtained by more complex calculations. The three most commonly used methods are the following:

1. Obtaining the fundamental phase voltage;
2. Using a PLL loop [10];
3. Detection of the voltage zero crossing.

For high immunity versus the voltage waveforms, the second method was adopted.

The PLL circuit has a specific structure (Fig. 4) and the implemented principle consists in canceling a fictitious instantaneous power [12].

$$p_f = u_a i_{af} + u_b i_{bf} + u_c i_{cf}, \qquad (4)$$

To the calculation of this power are introduced three fictitious currents (iaf, ibf, and icf) which meet the condition,

$$i_{af} + i_{bf} + i_{cf} = 0. \qquad (5)$$

The currents i_{af} and i_{cf} are reaction currents and are obtained on the basis of the voltage pulsation (ω) supplied by a PI controller.

Fundamental pulsation (ω_1) is obtained by filtering with a low-pass filter. After generating the signals and transforming them from the coordinate orthogonal system (α-β) into the three-phase system (a, b, c), the sinusoidal signals 1_{ula}, 1_{ulb} and 1_{ulc} result in phase with u_a, u_b and u_c fundamental voltages and amplitude equal to 1.

The main advantage is given by the permanent adaptation, both to variations in the amplitude of the voltages and to the frequency variations.

C. *Structure of the control system*

As a result of the authors' research, it was concluded that the best battery charging control strategy is the direct control of the AC current, as it allows obtaining unity power factor.

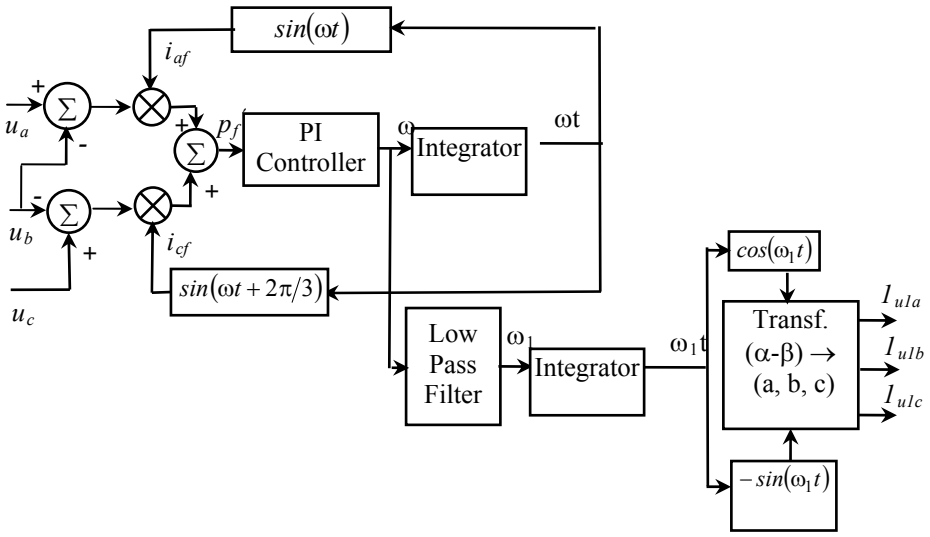

Fig. 4. Structure of the PLL circuit for the template of the grid current generating.

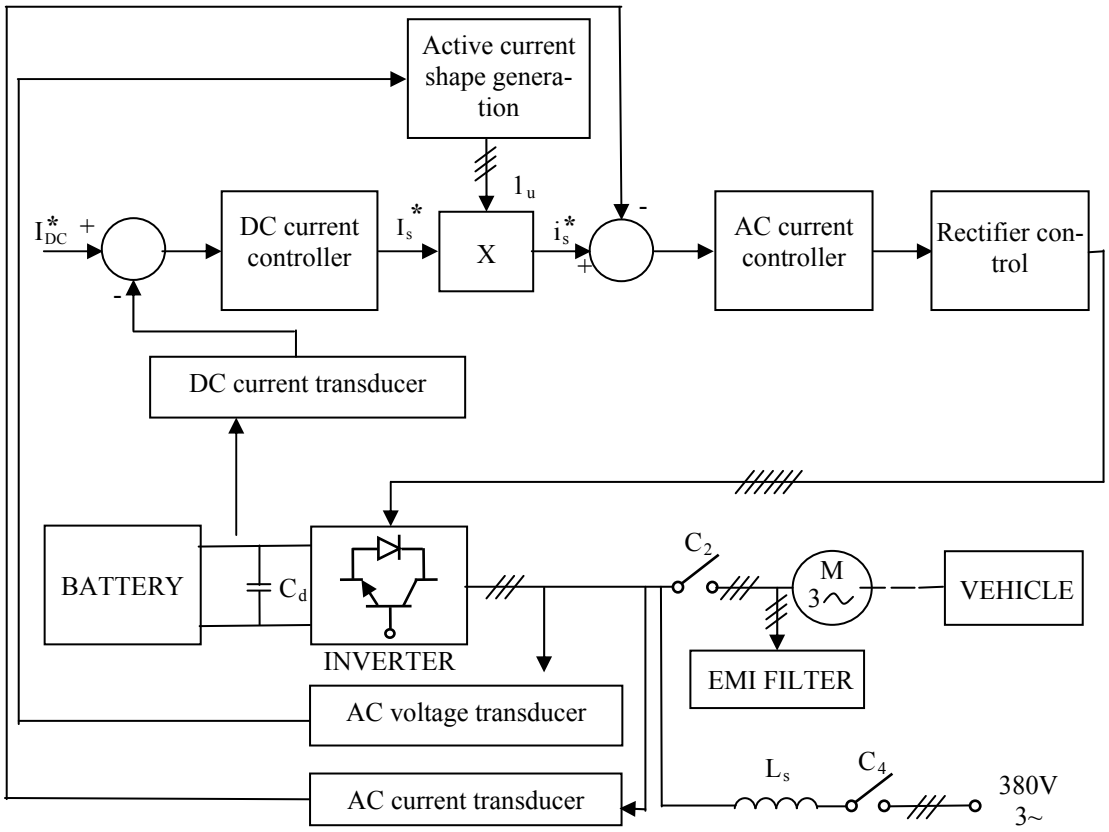

Fig. 5. Direct grid current control with two current loops.

Consequently, for implementation, the structure with two control loops is considered: an external loop for regulating the current on the DC side and an internal loop for adjusting the AC current (Fig. 5). Thus, the output of the DC current controller represents the prescribed amplitude of the grid current.

IV. The Transfer Functions and DC Current Controller Tunning

A. Operating equations

The operation equations are determined based on the single line diagram (Fig. 6). Thus, Kirchhoff's first law in the input node leads to:

$$i_s = i_c + i_2 \tag{6}$$

Applying the average values calculation operator to (6) gives:

$$\frac{1}{T}\int_0^T i_s dt = \frac{1}{T}\int_0^T i_c dt + \frac{1}{T}\int_0^T i_2 dt, \quad I_{sd} = I_{2d} \tag{7}$$

because the average value of the current through the filter capacitor is zero.

Considering the rectifier as a current source, the attached transfer function is:

$$\frac{I_0(s)}{I_{2d}(s)} = \frac{K_{iR}}{1+sT_{dy}}. \tag{8}$$

where K_{iR} is the rectifier transfer factor and T_{dy} is the delay time of the rectifier.

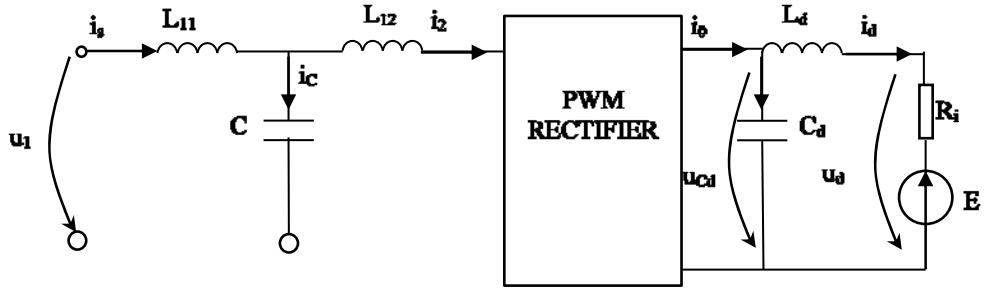

Fig. 6. Single line diagram of the battery charging system.

The Kirchhoff's first law in the output node leads to:

$$i_0 = i_{cd} + i_d \tag{9}$$

A second equation is obtained by applying Kirchhoff's second law on the output circuit, i.e.:

$$u_{cd} = R_t i_d + L_d \frac{di_d}{dt} + E. \tag{10}$$

The most unfavorable regime is then considered, when the open-circuit voltage of the battery is zero (E = 0).

Taking into consideration that

$$i_{cd} = C_d du_{Cd}/dt \tag{11}$$

expression (9) becomes:

$$i_0 = C_d du_{Cd}/dt + i_d \tag{12}$$

B. The operational scheme and the functional equations in the complex plan

The operational scheme corresponding to the adopted control scheme (Fig. 5) is obtained by adopting a hysteresis controller for the alternating current, which makes the transfer function of this loop to be considered unitary. In this way, the battery charging current control loop contains: the current controller whose output is the peak current of the network normalized in the range (0-10) V (I^*_{sn}); a current transformation block in real values (K_{Ti} is the proportionality constant of the current transducer); the transfer function $G_{ii}(s)$ between the peak current value of the network and the charge current of the battery.

After applying the Laplace transform to equations (10) and (12), the following expressions are obtained:

$$U_{cd}(s) = R_t I_d(s) + sL_d I_d(s) \tag{13}$$

$$I_0(s) = sC_d U_{Cd}(s) + I_d(s). \tag{14}$$

C. Transfer function beteween the peak grid current and battery charge current

Eliminating U_{cd}(s) between (13) and (14) results in the operational expression of the average output current:

$$I_0(s) = \left[sC_d R_t\left(1 + s\frac{L_d}{R_t}\right) + 1\right] I_d(s). \tag{15}$$

Then, the time constants are introduced, as follows:

$$T_{em} = \frac{L_d}{R_t};\ T_{ed} = C_d R_t. \tag{16}$$

In addition, the average phase current is replaced by the peak value,

$$I_{sd}(s) = \frac{2}{\pi} I_s(s). \tag{17}$$

Finally, the expression of the transfer function $G_{ii}(s)$ is:

$$G_{ii}(s) = \frac{I_0(s)}{I_s(s)} = \frac{2/\pi K_{iR}}{(1+sT_{dy})(1+sT_{ed}+s^2 T_{ed}T_{em})}. \tag{18}$$

The transfer factor of the rectifier is determined by expressing the output and input powers of the rectifier operating with unity power factor and neglecting the losses.

$$\begin{aligned} \sqrt{3}U_s I_s &= \sqrt{3}U_s \frac{\pi}{2\sqrt{2}} I_{sd} = U_d I_d \\ K_{iR} &= \frac{I_d}{I_{sd}} = \frac{\pi}{2}\sqrt{\frac{3}{2}}\frac{U_s}{U_d} \end{aligned} \tag{19}$$

To calculate the time constant T_{dy}, the following aspects regarding the control of the transistors are considered:

- The regulation refers to the average values of the current and, consequently, the control becomes effective only after a period of the current i_d (T/6 =1/(6f));
- In addition, depending on the control time of the transistors relative to the current period, there may also be a delay, due to the control period, which is between zero and $2T_{sw}$. Adopting the mean value of the delay means:

$$T_{dy} = 1/(6f) + 1/f_{sw}. \tag{20}$$

D. Synthesis of the current controller

Given the form of the fixed part transfer function $G_{ii}(s)$, a PI type controller is adopted, whose transfer function is:

$$G_{RId}(s) = (1 + s\theta_1)/s\theta. \tag{21}$$

In the transfer function (18), the product of the two time constants is very small and the corresponding term can be neglected. Thus, using the operational diagram of the bat tery charging current loop (Fig. 7), the transfer function of the fixed part is:

$$G_f(s) = \frac{1}{K_{Ti}} G_{ii}(s) = \frac{A_f}{(1+sT_{dy})(1+sT_{ed})}. \tag{22}$$

Total amplification has the expression:

$$A_f = \frac{1}{K_{Ti}}\frac{2}{\pi}K_{iR}. \tag{23}$$

The tuning is performed by the modulus criterion in Kessler variant, and therefore, the calculation algorithm is dependent on the ratio of the values of the two time constants that can be determined only after the design of the system. It is generally assumed that $T_{dy} >> T_{ed}$, because the internal resistance of the battery is of 10^{-3} order,

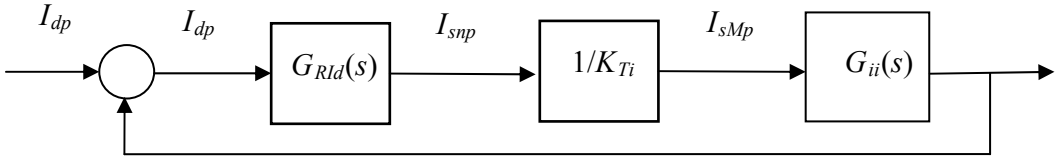

Fig. 7. Operational diagram of the battery charging current loop with unitary reaction.

the capacitance C_d is of 10^{-4} order and only the first component of T_{dy} is of order 10^{-3}.

Consequently, applying the modulus criterion, the dominant time constant (T_{dy}) is eliminated and the controller parameters are:

$$\theta_1 = T_{dy};\ \theta = 2A_f T_{sd} \tag{24}$$

V. Performances of the System

A. The Simulink Model

In order to determinate the performances of the system, the entire system was modeled under Simulink environment (Fig. 8).

The main parts of the model are:

- the power part that contains the grid, the PWM rectifier and its interface filter and the battery;
- the control part composed by d.c. current controller, a.c. current controller and IGBT's signals distribution block;
- the measure part composed by a lot of sensors;
- the monitoring and displaying part composed by a lot of oscilloscopes and numerical displays;
- the calculating part (average values, RMS values, harmonics, powers and switching frequency).

B. Results and performances

The performances are presented under graphical and numeric form and correspond of ramp prescribed charging current (Fig. 9).

The system response (Fig. 9) proves the proper synthesis of the controller. Thus, the charging current follows the prescribed values, has a little overshoot and the steady-state error is null.

These aspects are also reflected in the evolution of the output voltage and the charging current (Fig. 10). The proper operation of the hysteresis current controller is shown by evolutions of the peak grid current values, prescribed as the output of charging current controller and the real one (Fig. 11). They illustrate a very good performance during the steady-state regime. Practically, the instantaneous prescribed and real grid currents are identically (Fig. 12).

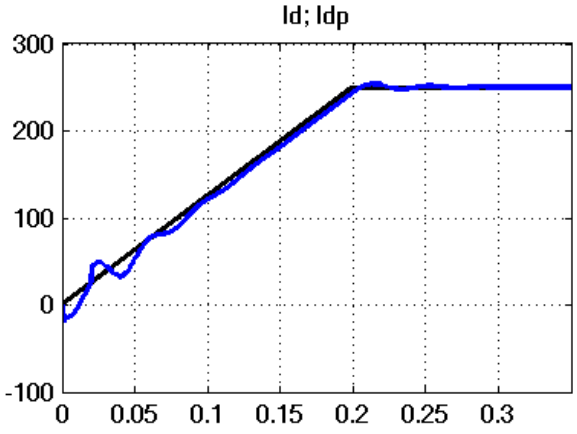

Fig. 9. The prescribed charging current (black) and real average charging current (blue).

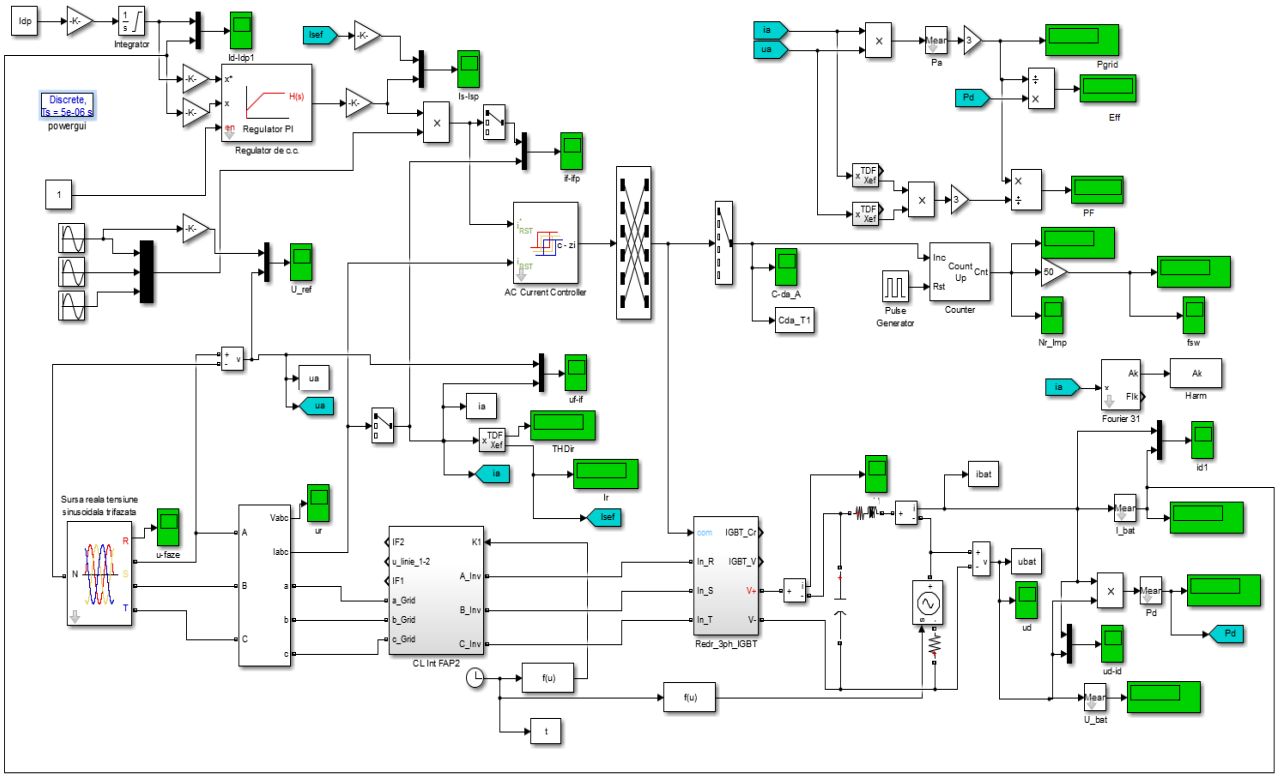

Fig. 8. The Simulink model of the control and power system.

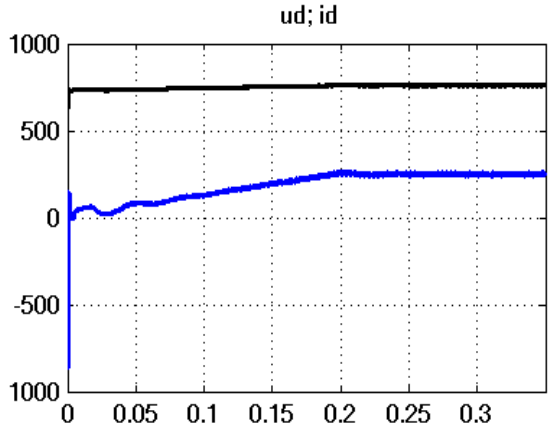

Fig. 10. The battery voltage (black) and current (blue).

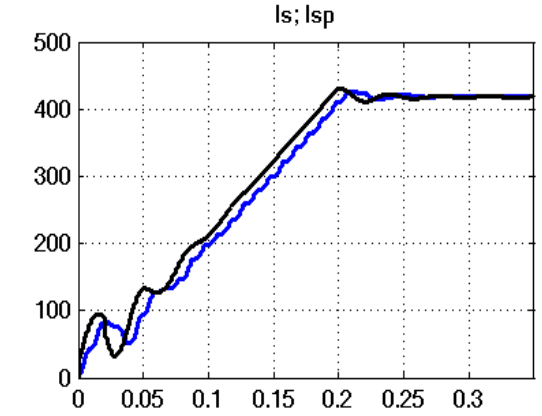

Fig. 11. The peak grid current: prescribed as controller output (black) and real (blue).

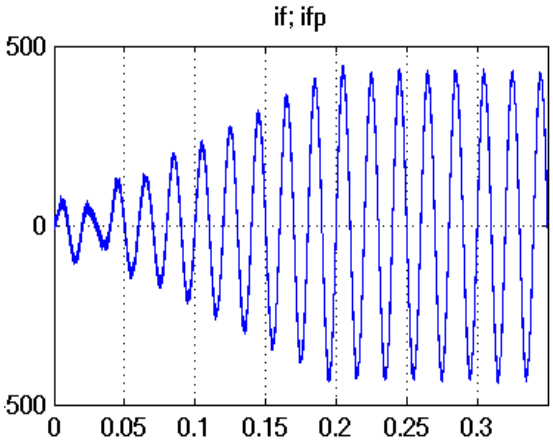

Fig. 12. The instantaneous grid current: prescribed (black) and real (blue).

The very good energetic performance is shown by the waveforms of the grid voltage and current (Fig. 13). Thus, the both are sinusoidal and their phases are the same.

TABLE I.
TABLE I. THE NUMERICAL VALUES OF THE MAIN ENERGETIC INDICATORS

P_{grid}[MW]	P_d[MW]	S_{grid}[MVA]	Eff[%]	PF[%]	Igrid[A]	THDIr[%]
0,1926	0,1897	0,192735	98,49	99,93	297	2,8

TABLE II.
THE MAIN PARAMETERS OF THE CHARGING SYSTEM

BATTERY			INVERTER		
U_N[V]	R_i[mΩ]	I_{charge}[A]	IGBT	C_d[μF]	Lgrid[mH]
800	120	250	CM1800DY	1700	3 x 0,5

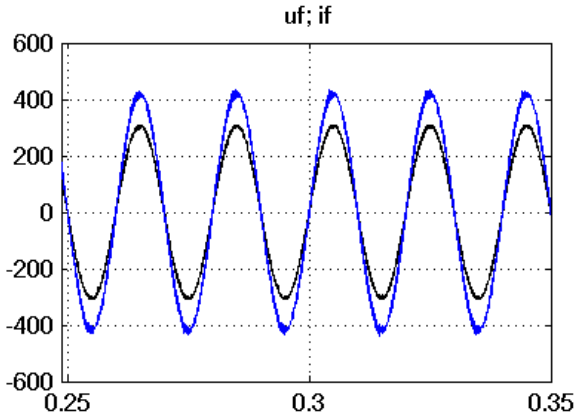

Fig. 13. The grid voltage (black) and current (blue)

VI. SWITCHING FREQUENCY INFLUENCE

To operate safely traction inverter transistors, research beneficiary has requested analysis of the influence of switching frequency and restricting it to 2 kHz.

By modifying the hysteresis threshold in the [0.1; 0.3] IN, switching frequency variation from 5.35 kHz to 1.95 kHz was obtained.

From the form point of view, the switching frequency influences the amplitude of the switching harmonics that overlap beyond to prescribed sinusoid (Fig. 14 and 15).

From the quantitative point of view, the current total harmonics distortion factor is strongly influenced. Thus, its values increase from 2.8% to 7.74% if switching frequency decreases from 5.35 kHz to 1.95 kHz (Fig. 16).

It is very important that the power factor is very low affected (Fig. 17). Thus, its value decreases from 99.93 % to 99.67 %.

This aspect shows that the switching frequency can be limited to 2 kHz without the energetically performances to be affected.

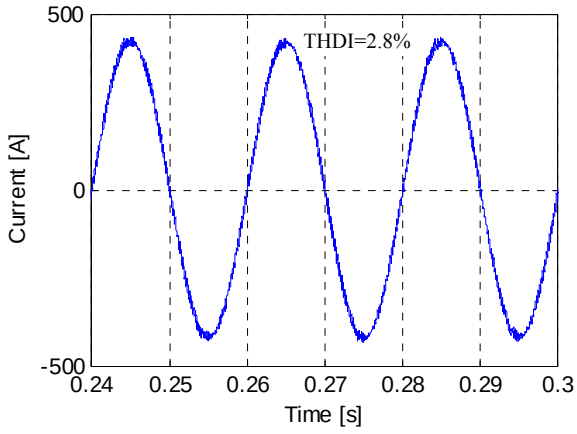

Fig. 14. The grid current corresponding to 5.35 kHz switching frequency

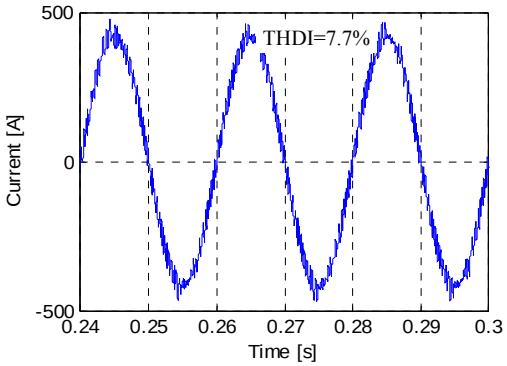

Fig. 15. The grid current corresponding to 1.95 kHz switching frequency

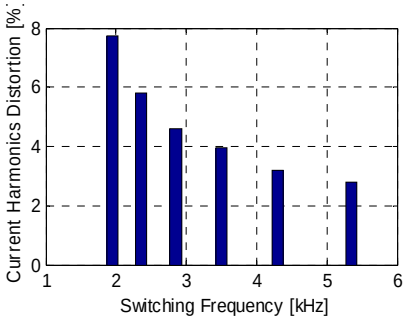

Fig. 16. Current Total Harmonics Distortion versus switching frequency

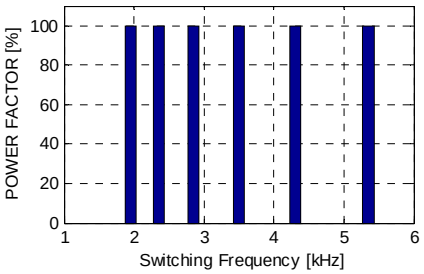

Fig. 16. Total Power Factor versus switching frequency

VII. Conclusions

1. The results obtained on the virtual system confirm the proper synthesis of the battery charging system dedicated to an electric stand-alone locomotive.

2. The virtual system corresponds to a real electric stand-alone locomotive.

3. The charging system uses the traction inverter operating as boost rectifier and the induction motor windings as interfacing inductivities.

4. The control part contains two current loops: the main one for the charging current control; the second for the grid current control.

5. The charging current controller was optimally tuned by the modulus criterion in Kessler variant.

6. Consequently, the dynamic and static performances are high.

7. The synthesized system operates with unity power factor and the grid current distortion falls within the required limits.

8. The variation of switching frequency from 5.35 kHz to about 2 kHz influences significantly only the harmonic distortion factor, but total power factor remains practically unchanged.

9. It is confirm the correctitude of system power structure and the control part and algorithm.

Acknowledgment

Source of research funding in this article: Project PACETSINEFEN POC-A1-A1.2.3–G2015, ID 40196, nr. 76/08.09.2016.

Contribution of authors:

Firs author – 50%

First coauthor – 20%

Second coauthor – 20%

Thirst Second coauthor – 10%.

Received on July 12, 2017

Editorial Approval on November 15, 2017

References

[1] A. Bitoleanu, M. Popescu, and V. Suru, ”Optimal controllers design in indirect current control system of active DC-traction substation,” in Proc. PEMC 2016, pp. 904-909, Sept. 2016.

[2] A. Bitoleanu, M. Popescu, and V. Suru, ”Theoretical and experimental evaluation of the indirect current control in active filtering and regeneration systems,” in Proc. OPTIM-ACEMP 2017, pp. 759-764, May 2017.

[3] A. Bitoleanu, Mihaela Popescu, V. C. Suru, F. A. Teodorescu - Synthesis of the Battery Charging System of a Stand-Alone Electric Locomotive Using the Traction Converter, 2018 International Conference on Applied and Theoretical Electricity (ICATE), Craiova, October 4-6, 2018.

[4] A. E.-Najar, M. A. Galiel, and H. A. Ashour, ”An efficient unity power factor battery charging/discharging unit,” in Proc. 2014 IEEE Innovative Smart Grid Technologies - Asia (ISGT ASIA).

[5] A. Bouafia and F.Krim, ”A fuzzy-logic-based controller for three-phase PWM rectifier with unity power factor operation”, J. Electrical Systems, 4-1, pp. 36-50, 2008.

[6] J. Chelladurai and B. Vinod, ”performance evaluation of three phase scalar controlled PWM rectifier using different carrier and modulating signal,” Journal of Engineering Science and Technology vol. 10, no. 4, pp. 420 – 433, 2015.

[7] I. Syed, M. Bala Subba Reddy, K. Hari Babu, ”Unity power factor control by PWM rectifier,” IJRET, vol. 2 issue 10, Oct. 2013.

[8] J. Lamterkati, M. Khafallah, and L. Ouboubker, ”A new DPC for three-phase PWM rectifier with unity power factor operation,” IJAREEIE, vol. 3, issue 4, April 2014.

[9] M. Xue and M. He, ”Control of unit power factor PWM rectifier,” Energy and Power Engineering, pp. 121-124, 2013.

[10] M. Popescu, A. Bitoleanu, and A. Preda, ”A new design method of an LCL filter applied in active DC-traction substations”, IEEE Trans. Ind. Appl., vol. 54, issue 4, pp. 3497-3507, July/Aug. 2018.

[11] M. Rădulescu, “Electric Drive and Battery-Charging Power Electronic System,” International Patent WO/2011/055230.

[12] M. Popescu, A. Bitoleanu, and V. Suru, ”A DSP-based implementation of the p-q theory in active power filtering under nonideal voltage conditions”, IEEE IEEE Trans. Ind. Inf., vol. 9, issue 2, pp. 880-889, May, 2013.

[13] Q.-C. Zhong, Z. Ma and P.-L. Nguyen, “PWM-controlled rectifiers without the need of an extra synchronisation unit,”, In Proc. IECON 2012, Oct. 2012.

[14] Z. Zeng, W. Zheng, R. Zhao, C. Zhu, and Q. Yuan, ”Modeling, modulation, and control of the three-phase four-switch PWM rectifier under balanced voltage,” IEEE Trans. Power Electron., vol. 31, issue 7, pp. 4892 – 4905, July 2016.

[15] Z. Ma, D. Xu, R. Li, C. Du, and X. Zhang, ”A novel DC-side zero-voltage switching (ZVS) three-phase boost PWM rectifier controlled by an improved SVM method”, IEEE Trans. Power Electron., vol. 27, issue 11, Nov. 2012, pp. 4391 – 4408.